PROCEEDINGS, 49th Workshop on Geothermal Reservoir Engineering
Stanford University, Stanford, California, February 12-14, 2024
SGP-TR-227

3D Seismic Imaging and Fault Detection at the Lightning Dock Geothermal Field

Lianjie Huang[1], Kai Gao[1], David Li[1], Chenglong Duan[1], Trenton Cladouhos[2], Yingcai Zheng[3], Boming Wu[3], and Michael Swyer[4]

[1]Los Alamos National Laboratory, Los Alamos, NM 87545; [2]Stoneway Geothermal, Seattle, WA 98103; [3]University of Houston, Houston, TX 77004; [4]Cyrq Energy, Inc., Reno, NV 89520

ljh@lanl.gov

Keywords: Fault detection, first-arrival traveltime tomography, full-waveform inversion, Lightning Dock geothermal field, machine learning, reverse-time migration, siting geothermal wells.

ABSTRACT

New wells are often needed to improve energy production in geothermal power plants. Integrating 3D seismic imaging and fault detection with geological and geochemical information can help site new geothermal injection wells to reduce drilling risk and ensure the sustainability of geothermal power production. Lightning Dock Geothermal (LDG) LLC conducted a 3D active-source surface seismic survey in 2011 using accelerated weight drop sources for subsurface characterization. We use an open-source data analysis package called Madagascar to process the raw seismic data, update the velocity model in the shallow region using first-arrival traveltime tomography, improve the entire 3D surface velocity model using full-waveform inversion, and produce a 3D subsurface image of the Lightning Dock geothermal field using reverse-time migration. We then detect faults on the 3D seismic image using a machine learning algorithm based on nested residual U-Net. Our 3D seismic imaging and fault detection results provide valuable information for siting new geothermal wells at the Lightning Dock geothermal field.

1. INTRODUCTION

The Lightning Dock geothermal (LDG) power generating station is in Hidalgo County, southwest New Mexico, USA. The power plant began operations in late 2013 with 4 MW of electricity generation. In 2018, the field expanded by adding a new geothermal production well and a new power plant, reaching 12 MW of electricity generation.

Additional injection wells are desired to return cooled geothermal water to the Lightning Dock geothermal reservoir. To effectively site injection wells, the subsurface structure must be well-characterized to locate the ideal combination of faults, formation permeability, connectivity between wells, and temperature. Gao et al. (2022a) imaged geothermal flow using a long-duration passive seismic signals recorded with a large-N array consisting of 1,206 nodal geophones at the Lightening Dock geothermal field. 3D imaging of active seismic data and fault detection on a migration image can provide useful additional information for site new geothermal wells because geological faults often act as pathways of geothermal fluids.

LDG LLC conducted a 3D active-source surface seismic survey in 2011 using accelerated weight drop sources for subsurface characterization. The 3D seismic survey covered a region of approximately 4 km in the east-west direction and approximately 3.5 km in the north-south direction, as shown in Figure 1. This 3D seismic survey used a simple box pattern to distribute sources and receivers. The survey used a total of 17 receiver lines with a quasi-equal spacing of 660 ft and with an orientation of north-south, and a total of 21 source lines with a quasi-equal spacing of 600 ft and with an orientation of east-west. Within the source lines or the receiver lines, the source interval is 110 ft and the receiver interval is 220 ft. The data acquisition was conducted in a spreading-roll configuration, and therefore, each common-shot gather covers different regions of the entire seismic survey area. The dataset contains a total of 1,965 spreading-roll 3D common-shot gathers.

The recording geometry consists of a total of 984 Sunfill PS-14B (14 Hz) geophones with four geophones per string potted together on station flag, and a total of 2,168 sources with each source being a single truck-mounted DigiPulse 1180 accelerated weight drop unit. This type of source produces a strong impulsive, broadband seismic signal. The survey was recorded with a Seistronix EX-6 recording system. The seismic data were recorded with a 2-ms temporal sample rate, and the record length was 3 s. Our data extraction and processing result in a total of 1,965 usable common-shot gathers.

We use an open-source data analysis package called Madagascar (https://www.reproducibility.org/wiki/Main_Page) to process the raw 3D seismic data. We attenuate ground-roll noises, pick the first-arrival traveltimes on the seismic traces, and update the velocity model in the shallow region using 3D surface-source first-arrival traveltime tomography (FATT). To further improve of the entire 3D surface velocity model for seismic migration, we perform 3D full-waveform inversion (FWI) of the seismic data. We then apply reserve-time migration to the seismic data to produce a 3D subsurface image of the Lightning Dock geothermal field. Finally, we delineate faults on the 3D migration image using a machine learning method based on nested residual U-Net (Gao et al., 2022b). Our results show that the

west part of the Lightning Dock geothermal field develops more geological faults compared with the east part of the region. Our imaging and fault detection results provide valuable information to reduce the drilling risk of future geothermal wells and increase geothermal production at the Lightning Dock geothermal field.

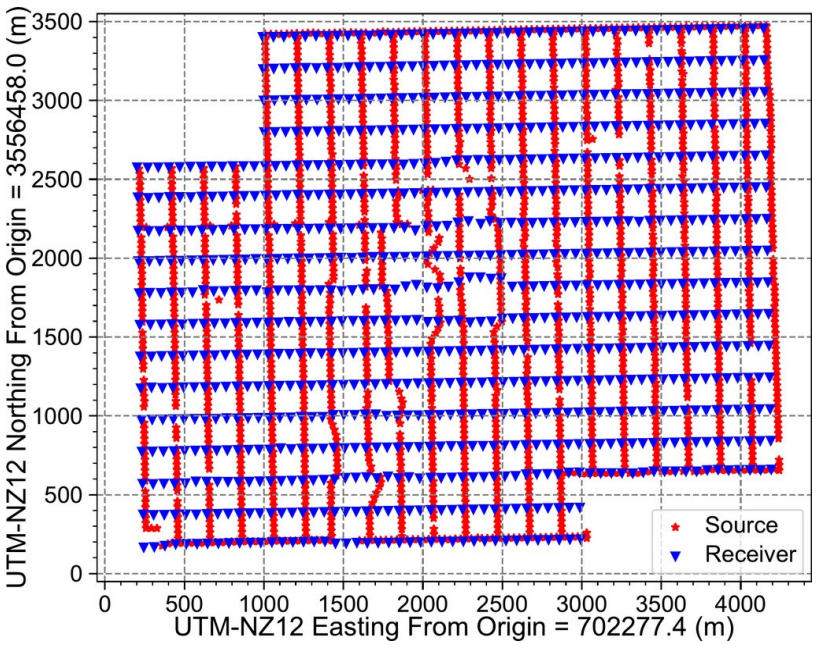

Figure 1: The distribution of sources and receivers of the 3D active-source surface seismic survey at the Lightning Dock geothermal field conducted in 2011.

2. METHODOLOGY

We perform seismic data processing using the Madagascar software package, pick first-arrival traveltimes, perform 3D surface active-source first-arrival traveltime tomography, implement 3D full-waveform inversion and 3D reverse-time migration, and detect faults on the 3D migration image using machine learning.

After processing the 3D active-source surface seismic data from the Lightning Dock geothermal field, we pick traveltimes of the first arrivals on the common-shot gathers for first-arrival traveltime tomography. Because of the large volume of the seismic data, we pick the first-arrival traveltimes using the following hybrid manual and automatic picking procedure. First, we estimate synthetic first arrival traveltimes using an initial velocity model and use these synthetic first-arrival traveltimes as a guide for picking our initial picks on common-shot gathers. We then employ short-time average over long-time average (STA/LTA) within a short time window of seismic traces around the synthetic first-arrival traveltimes as a guide for each common-shot gather. We omit STA/LTA results that are too far off from the synthetic results and manually pick the first-arrival times that we omit. We then use the STA/LTA and manual picks to select a time window for the traces that contain the first arrivals and perform a deconvolution to obtain zero-phase traces. Finally, we automatically select the troughs on the zero-phase traces to reduce uncertainty in our picks.

With the picked first-arrival traveltimes, we use adjoint-state first-arrival traveltime tomography (Leung and Qian, 2006; Taillandier et al., 2009) to perform velocity update in the shallow region of the Lightning Dock geothermal field. The method minimizes a traveltime misfit function with respect to the P-wave velocity model. We employ the second-order fast-marching method to solve the eikonal equation for ray tracing. We solve the minimization problem using the conjugate-gradient (CG) method (Nocedal and Wright, 2006) and compute the optimal step size in each iteration using a small perturbation strategy (Gauthier et al., 1986).

After first-arrival traveltime tomography, we employ full-waveform inversion (FWI) to further improve the entire subsurface velocity model. FWI is a nonlinear minimization problem to seek an optimal set of subsurface medium property models by minimizing the misfit between the synthetic and field seismic waveforms (Tarantola, 1984). FWI is highly nonlinear and generally difficult to converge because of the issues of cycle skipping and unknown source wavelets, particularly for noisy field seismic data and complex subsurface structures and/or properties (Virieux and Operto, 2009; Vigh et al., 2014; Warner and Guasch, 2016). We employ a normalized deconvolution misfit function to improve the convergence of FWI (Warner and Guasch, 2016). Studies show that this deconvolution-based misfit function usually results in notably better convergence and reliable inversion results compared with FWI based on the conventional L_2-norm waveform misfit function.

With the FWI-updated velocity model, we apply 3D reverse-time migration (RTM) to the processed seismic data to obtain a high-resolution subsurface image. RTM is an advanced imaging technique for imaging complex structures (McMechan, 1983; Chang and McMechan, 1987). RTM uses full waveforms to form subsurface images, capable of handling complex subsurface structures. Seismic migration usually forms a migration image using an imaging condition based on zero time-lag cross-correlation between the forward-propagated source pressure wavefield and the back-propagated receiver pressure wavefield. To attenuate low-wavenumber artifacts in the RTM image, we employ an implicit wavefield separation-based imaging condition (Fei et al., 2015). We obtain the subsurface structural image by stacking the images generated using all common-shot gathers after properly tapering and balancing individual common-shot gather images.

The complexity of the subsurface image motivates us to perform an automatic seismic fault detection using a machine-learning-based fault detection method (Gao et al., 2022b). The method uses a nested residual U-shaped convolutional neural network. Each of the encoders and decoders in this neural network is a residual U-Net, resulting in a nested architecture. The method produces a fault system by fusing three fault maps with low, medium, and high fault resolutions.

3. RESULTS

The 3D seismic data of the Lightning Dock active-source seismic survey were originally stored in the SEG-2 format with separate files describing the source-receiver configurations. To facilitate our research, we convert the SEG-2 data to the SEG-Y format by extracting trace data and source-receiver geometry relations from the relevant files. Figure 2(a) and Figure 3(a) shows two examples of common-shot gathers of the 3D seismic data, showing that the data contain strong ground-roll noises, random noises, and coherent noises.

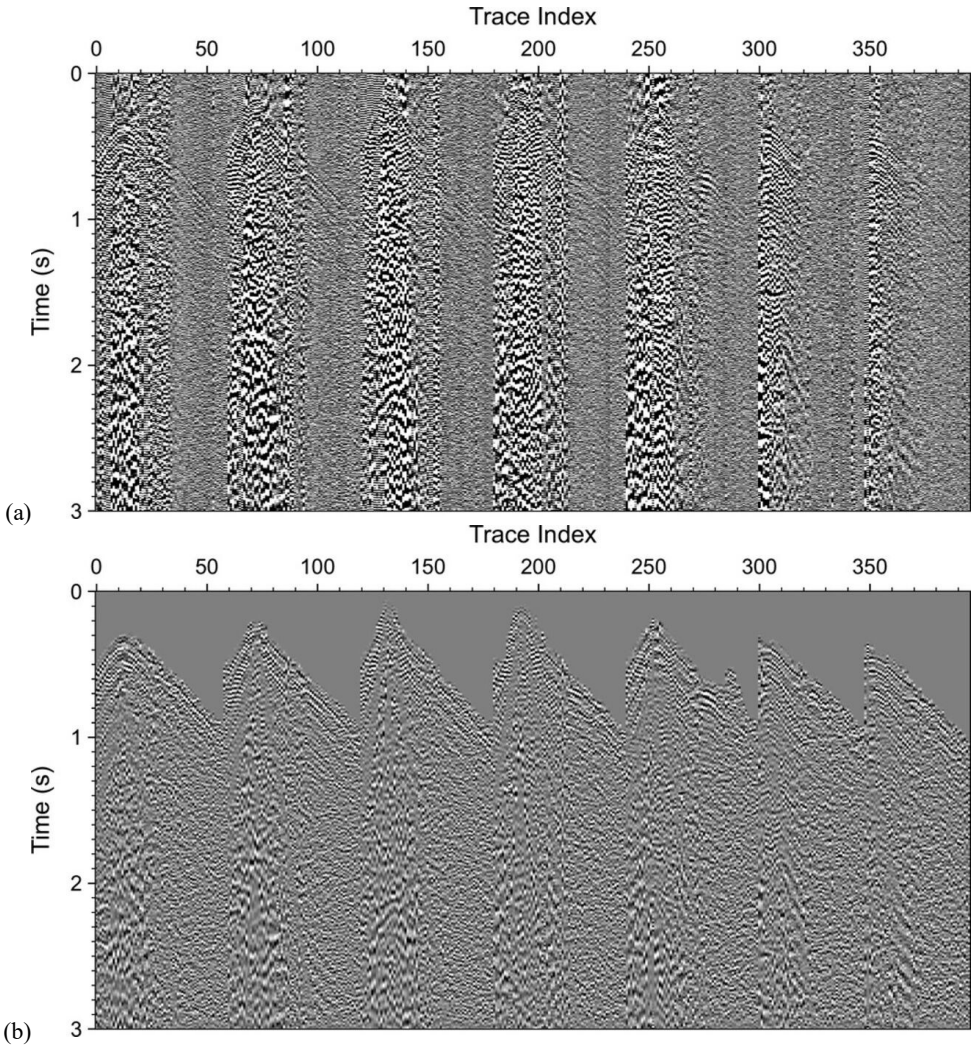

Figure 2: (a) An example common-shot gather of the Lightening Dock 3D active seismic data, and (b) the same common-shot gather after LANL's seismic data processing.

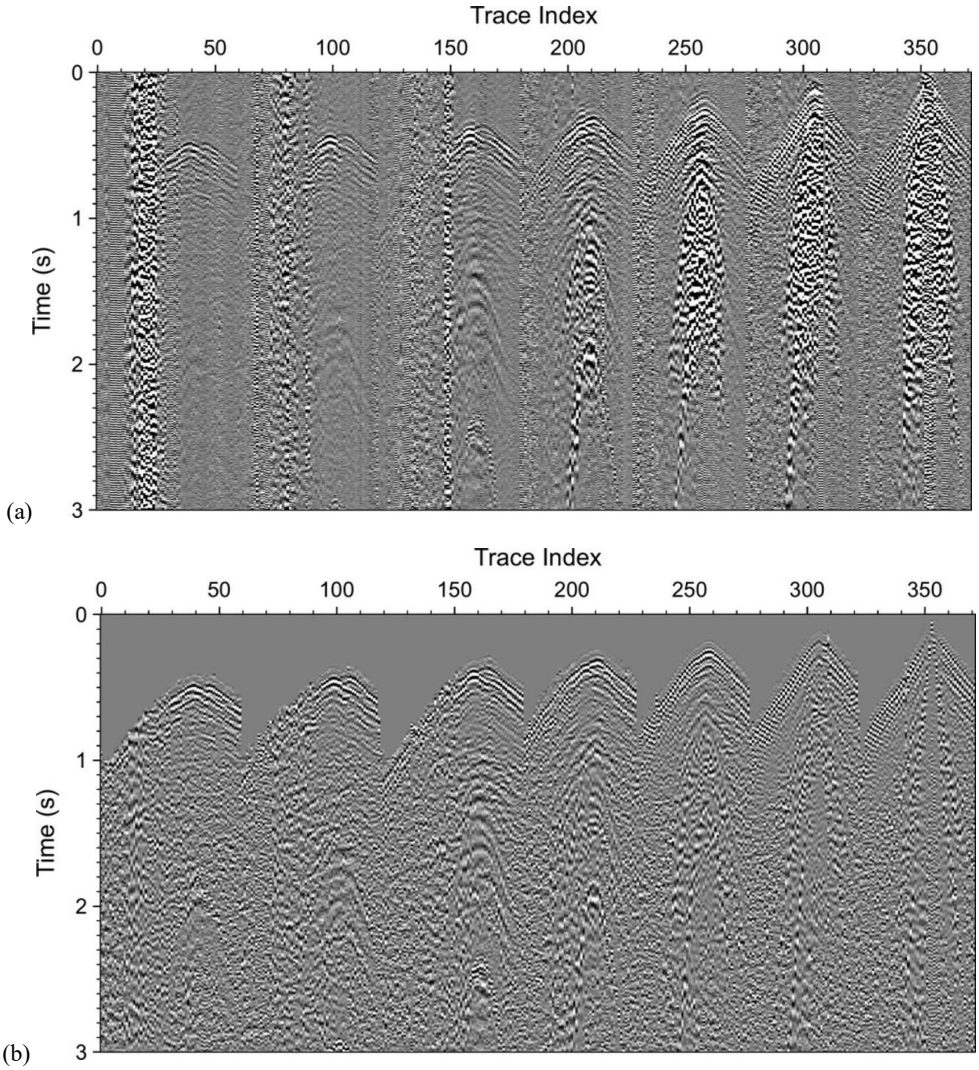

Figure 3: (a) Another example common-shot gather of the LDG 3D active seismic data, and (b) the same common-shot gather after LANL's seismic data processing.

We process the Lightning Dock 3D seismic data using Madagascar, an open-source software package for multidimensional data analysis. We attenuate strong ground-roll signals and random noises, mute the seismic traces before the first-arrival signals, band-pass filter to remove low- and high-frequency components, and balance the seismic traces. Figure 2(b) and Figure 3(b) display the processed seismic data corresponding to the two example common-shot gathers in Figure 2(a) and Figure 3(a), respectively. Figure 2 and Figure 3 show that, after our seismic data processing, the ground-roll noises are mostly suppressed, the far-offset traces become more energy-balanced compared with those in the raw data, and the signal-to-noise ratios of the data are notably increased. Nevertheless, additional refined seismic data processing could improve the data quality for subsurface imaging and fault detection.

We pick first-arrival traveltimes of all common-shot gathers using our hybrid manual and automatic picking procedure. We then use the picks to perform 3D surface active-source first-arrival traveltime tomography. The 3D surface active-source FATT updates the initial velocity model obtained using the string-shot FATT as shown in Figure 4(a) (Gao et al., 2022a). A borehole active-source seismic survey (reverse vertical seismic profiling) was conducted using seven string shots in existing geothermal wells at the Lightning Dock geothermal field and the data were recorded using a surface large-N array. An initial velocity (Vp) model was derived using FATT of the string-shot seismic data (Gao et al., 2022a).

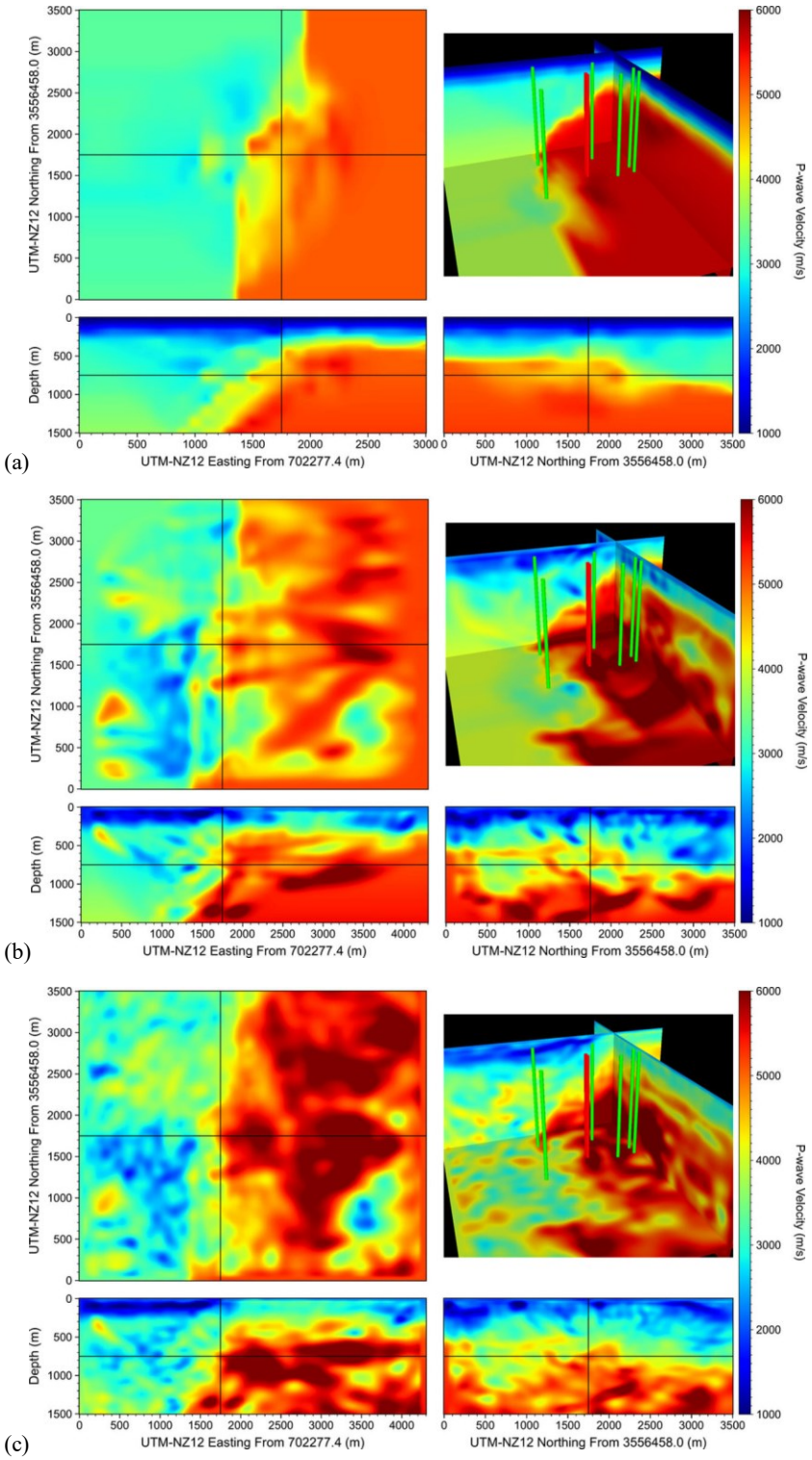

Figure 4: (a) The initial P-wave velocity model obtained using first-arrival traveltime tomography of the string-shot seismic data acquired using the large-N array (Gao et al. 2022a); (b) The P-wave velocity model produced using LANL's FATT; and (c) The P-wave velocity model produced using LANL's full-waveform inversion of the processed common-shot gathers of the Lightning Dock 3D surface active seismic data. The green tubes are active injection wells, and the red tubes are active geothermal production wells.

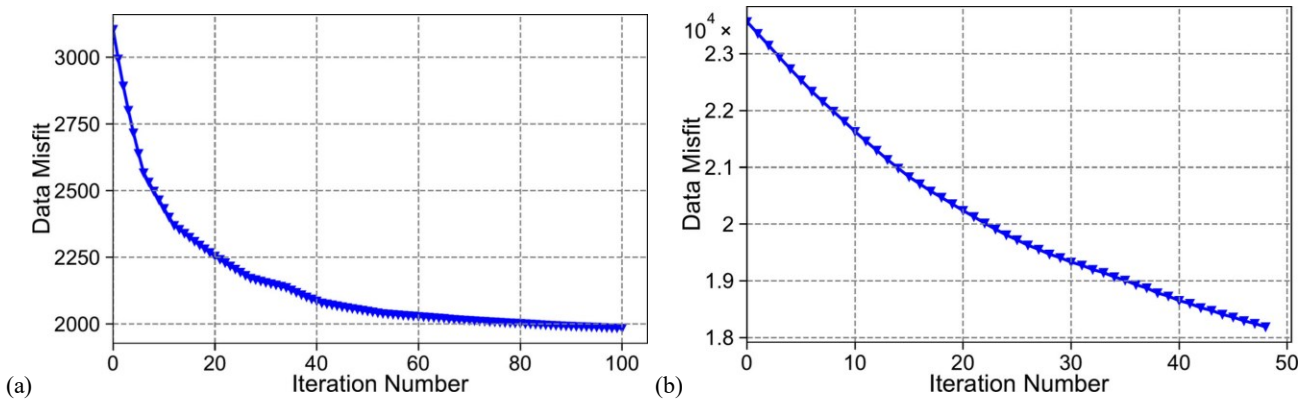

Figure 5: The misfit convergence curves of (a) 3D active-source first-arrival traveltime tomography and (b) 3D FWI of the Lightning Dock 3D surface active seismic data.

Compared with the string-shot FATT velocity model in Figure 4a, our 3D surface active-source FATT velocity model in Figure 4(b) has a higher spatial resolution. This higher spatial resolution results from the better coverage of sources and receivers in the 3D active-source surface seismic survey with 1,965 common-shot gathers compared with seven common-shot gathers in the string-shot data. The general structure of the velocity model in Figure 4(b) is similar to that in Figure 4(a), yet we find that there are more details revealed by our 3D surface active-source FATT. For example, on the right (east) part of the model, the surface active-source FATT velocity model reveals some heterogeneities within the high-velocity geological block, while in the string-shot FATT velocity model, this high-velocity block is only slightly heterogeneous. The left (west) part of the 3D surface active-source FATT velocity model also shows more heterogeneities compared with that in the string-shot FATT velocity model.

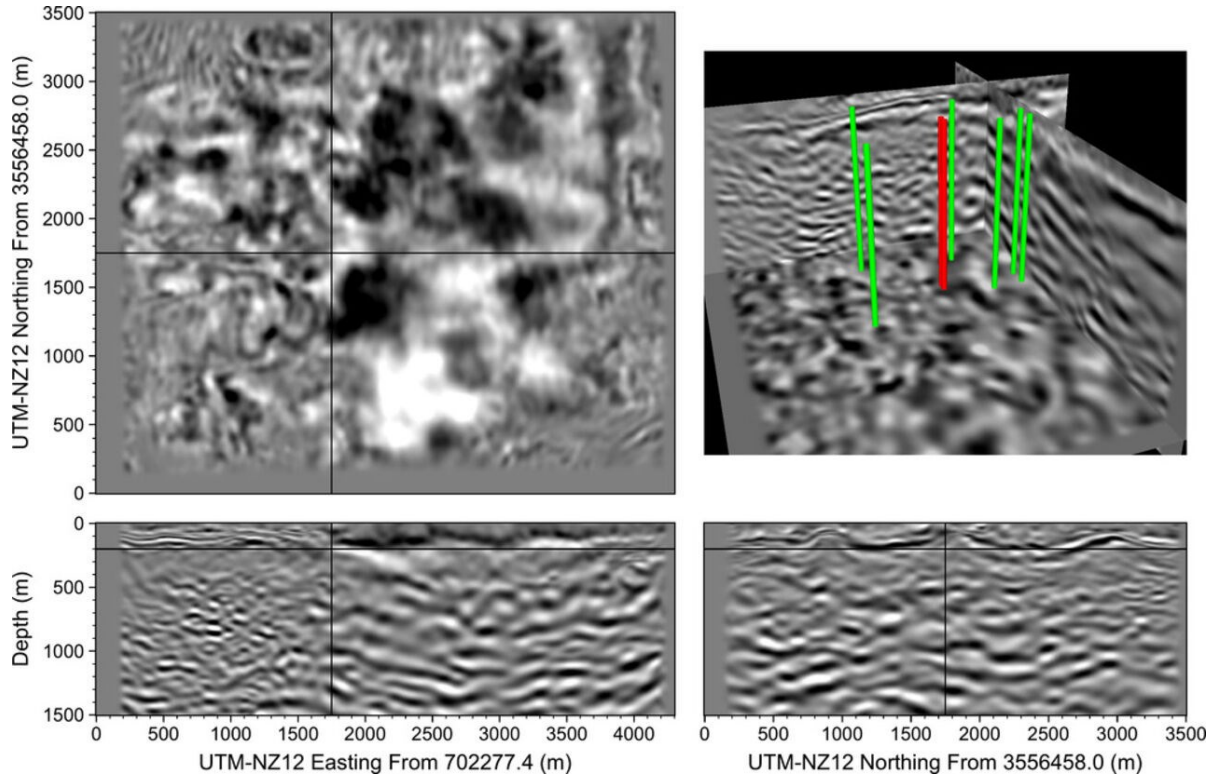

Figure 6: The 3D migration image produced using LANL's wavefield-separation-based reverse-time migration of the Lightning Dock 3D surface active seismic data.

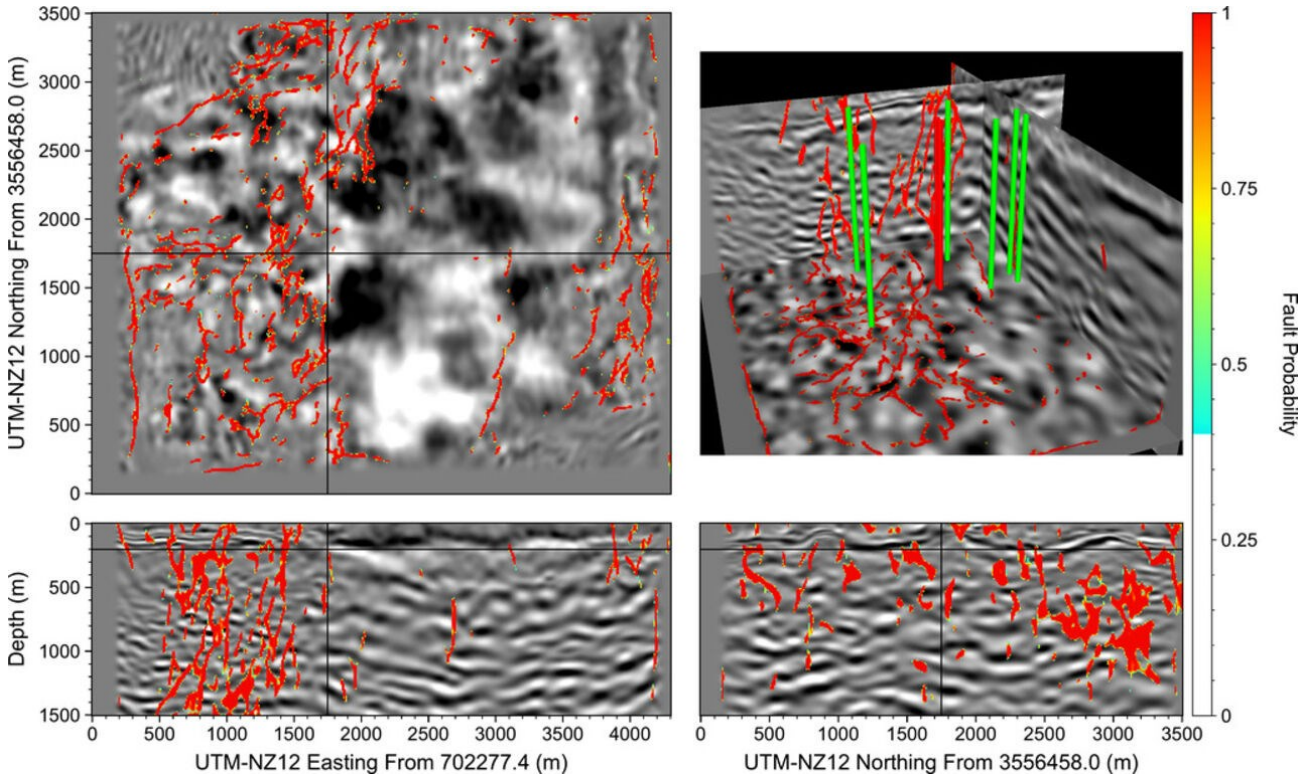

Figure 7: Faults detected on the 3D migration image in Figure 6 using LANL's machine-learning-based automatic fault detection method, overlaying on the migration image. The color shows the probability of the detected faults.

Using our 3D surface active-source FATT velocity model in Figure 4(b) as the initial model, we perform 3D full-waveform inversion using the normalized deconvolution misfit function and obtain the FWI velocity model in Figure 4(c). FWI further improves the spatial resolution of the velocity model. In both the east and west blocks in Figure 4(c), FWI reveals more finer heterogeneities compared with the FATT velocity model in Figure 4(b). In the deeper region, the FWI velocity model also reveals complex velocity heterogeneities that correspond to the complex, non-coherent scattering and reflections contained in the Lightning Dock 3D active seismic data. The FWI velocity model indicates that, in addition to the major geological fault in the center of the model spanning from north to south, there exist other complex heterogeneities in the subsurface of the Lightning Dock geothermal field.

Figure 5 shows the misfit convergence curves for our 3D surface active-source FATT in Figure 5(a) and 3D FWI in Figure 5(b), respectively. They both converge well, indicating the reliabilities of our 3D FATT and FWI results.

Using the 3D FWI velocity model in Figure 4(c), we perform 3D structural imaging using the wavefield-separation-based reverse-time migration of the 3D surface seismic data and produce the 3D migration image in Figure 6. We find that the shallow reflectors in the image volume is relatively stronger and more continuous than those in the deeper part of the image. Particularly, we observe a strong reflector at the depth of 200 to 400 m below the ground surface. In the deep region of the image volume, most of the reflectors are discontinuous in the horizontal direction, resulting in difficulties in geological interpretation.

Finally, we delineate the 3D fault system on the migration image in Figure 6 using a nested residual U-Net. Figure 7 displays the predicted faults overlaying on the RTM image volume. The colors represent the fault probability output of the machine learning algorithm, and the red color represents the high fault probability. The machine-learning fault detection algorithm detects more geological faults in the left part of the image as displayed in the horizontal slice plot in Figure 7, and most of these faults orient in the north-south direction. The east block with higher velocities (the right part of the image) contains a fewer number of faults compared with the west block with lower velocities (the left part of the image). The abundant discontinuities in the image volume introduce great challenges to automatic fault detection algorithms. For reliable fault detection, we need to acquire higher-quality seismic data, refine seismic data processing, and produce a higher-resolution, higher-quality subsurface image. In addition, we can use least-squares reverse-time migration and machine-learning-based image denoising (Huang et al., 2023) to obtain higher-quality subsurface images.

4. CONCLUSIONS

We have performed 3D first-arrival traveltime tomography, full-waveform inversion, reverse-time migration, and fault detection using the 3D surface seismic data acquired at the Lightning Dock geothermal field for subsurface characterization. The FWI velocity model reveals more fine-scale heterogeneities at the Lightning Dock geothermal field, indicating the geological complexity of this area. The 3D image volume shows that there are a great number of lateral discontinuities in this region, and continuous sedimentary layers are only visible in the shallow part of the region. We have performed machine-learning-based automatic fault detection on the 3D migration image to delineate the complex fault system at the Lightning Dock geothermal field. The results show that the left (west) part of the region develops more geological faults compared with the right (east) part of the region. Our 3D imaging and fault detection results provide valuable information for siting new geothermal wells to reduce drilling risks and increase geothermal production at the Lightning Dock geothermal field. Acquiring higher-quality seismic data, refining seismic data processing, and enhancing imaging quality can further improve the reliability of fault detection.

ACKNOWLEDGMENTS

This work was supported partially by The New Mexico Small Business Assistance (NMSBA) Program and partially by the U.S. Department of Energy (DOE) Geothermal Technologies Office through the Los Alamos National Laboratory (LANL), which is operated by Triad National Security, LLC, for the National Nuclear Security Administration (NNSA) of U.S. DOE under Contract No. 89233218CNA000001. This research used resources provided by the LANL Institutional Computing Program, which is supported by the U.S. DOE NNSA under Contract No. 89233218CNA000001.

REFERENCES

Chang, W.-F., and McMechan, G. A.: Elastic reverse-time migration, Geophysics, 52, no. 10, 1365–1375, doi: 10.1190/1.1442249 (1987).

Fei, T., Luo, Y., Yang, J., Liu, H., and Qin, F. Removing false images in reverse time migration: The concept of de-primary, Geophysics, 80, no. 6, S237–S244, doi: 10.1190/ geo2015-0289.1 (2015).

Huang, L., Gao, K., Li, D., Zheng, Y., and Cladouhos, T.: Delineating Faults beneath Basalt at the Soda Lake Geothermal Field, Proceedings, 48th Workshop on Geothermal Reservoir Engineering, Stanford University, Stanford, CA (2023).

Gao, K., Huang, L., Edwards, J., and Claduohos, T.: Monitoring Geothermal Flow at the Lightning Dock Geothermal Area, New Mexico Using Long-Duration Passive Seismic Imaging, Proceedings, 47th Workshop on Geothermal Reservoir Engineering, Stanford University, Stanford, CA (2022a).

Gao, K., Huang, L., and Zheng, Y.: Fault detection on seismic structural images using a nested residual U-Net, IEEE Transactions on Geoscience and Remote Sensing, 60, 1–15, doi: 10.1109/TGRS.2021.3073840 (2022b).

Gauthier, O., Virieux, J., and Tarantola, A.: Two-dimensional nonlinear inversion of seismic waveforms: Numerical results, Geophysics, 51, no. 7, 1387–1403, doi: 10.1190/1. 1442188 (1986).

Leung, S., and Qian, J.: An adjoint state method for three-dimensional transmission traveltime tomography using first-arrivals, Communications in Mathematical Sciences, 4, no. 1, 249–266 (2006).

McMechan, G. A.: Migration by extrapolation of time-dependent boundary values, Geophysical Prospecting, 31, no. 3, 413–420, doi: 10.1111/j.1365-2478.1983. tb01060.x (1983).

Nocedal, J., and Wright, S. J.: Numerical Optimization, 2 ed., Springer, New York (2006).

Taillandier, C., Noble, M., Chauris, H., and Calandra, H.: First-arrival traveltime tomography based on the adjoint-state method, Geophysics, 74, no. 6, WCB1–WCB10, doi: 10.1190/ 1.3250266 (2009).

Tarantola, A.: Inversion of seismic reflection data in the acoustic approximation, Geophysics, 49, no. 8, 1259–1266, doi: 10.1190/1.1441754 (1984).

Vigh, D., Jiao, K., Watts, D., and Sun, D.: Elastic full-waveform inversion application using multicomponent measurements of seismic data collection, Geophysics, 79, no. 2, R63–R77, doi: 10.1190/geo2013-0055.1 (2014).

Virieux, J., and Operto, S: An overview of full-waveform inversion in exploration geo- physics, Geophysics, 74, no. 6, WCC1–WCC26, doi: 10.1190/1.3238367 (2009).

Warner, M., and Guasch, L.: Adaptive waveform inversion: Theory, Geophysics, 81, no. 6, R429–R445, doi: 10.1190/geo2015-0387.1 (2016).